Rotation suppresses giant-scale solar convection

Geoffrey M. Vasil[a,1], Keith Julien[b], and Nicholas A. Featherstone[b,c]

[a]School of Mathematics and Statistics, University of Sydney, Sydney, NSW 2006, Australia; [b]Department of Applied Mathematics, University of Colorado, Boulder, CO 80309-0526; and [c]Department of the Space Studies, Southwest Research Institute, Boulder, CO 80302

Edited by Neta A. Bahcall, Princeton University, Princeton, NJ, and approved May 4, 2021 (received for review October 28, 2020)

The observational absence of giant convection cells near the Sun's outer surface is a long-standing conundrum for solar modelers. We herein propose an explanation. Rotation strongly influences the internal dynamics, leading to suppressed convective velocities, enhanced thermal-transport efficiency, and (most significantly) relatively smaller dominant length scales. We specifically predict a characteristic convection length scale of roughly 30-Mm throughout much of the convection zone, implying weak flow amplitudes at 100- to 200-Mm giant cells scales, representative of the total envelope depth. Our reasoning is such that Coriolis forces primarily balance pressure gradients (geostrophy). Background vortex stretching balances baroclinic torques. Both together balance nonlinear advection. Turbulent fluxes convey the excess part of the solar luminosity that radiative diffusion cannot. We show that these four relations determine estimates for the dominant length scales and dynamical amplitudes strictly in terms of known physical quantities. We predict that the dynamical Rossby number for convection is less than unity below the near-surface shear layer, indicating rotational constraint.

solar convection | Rossby number | rapid rotation | differential rotation

Turbulent thermal convection dominates the energy transport throughout the Sun's outer envelope. In recent years, puzzling disagreements have arisen between observations, models, and theory regarding the amplitude and structure of convection (1–3). Some work has begun to address the situation (4, 5). However, the discrepancy is not settled and has come to be called the convective conundrum (6).

In this paper, we demonstrate how the dominant dynamical balances in the solar interior make first-principle predictions for the spatial scale and amplitude of deep solar convection. Our analysis shows that interior flows likely exist in a quasigeostrophic (QG) state, with a joint Coriolis–inertial–Archimedean (CIA) balance (e.g., refs. 7–10) remaining after accounting for leading-order geostrophy.* Rotation strongly influences solar convection as a result. Our results put on a firm theoretical footing the earlier suggestions of Miesch et al. (4) and Featherstone and Hindman (5). We also corroborate and provide context to the observations of Hanasoge et al. (1, 3), as well as more recent observations (11). Our estimates leave the flow amplitude only somewhat smaller than previous mixing-length models, which ignore rotational effects. However, we demonstrate that rotational influence in the Sun most prominently affects the dominant flow length scale.

1. Solar Convective Processes

Apart from negligible friction, a turbulent fluid conserves angular momentum as it traverses the solar envelope. Angular-momentum transport occurs throughout the interior and generates differential rotation comprising a fast equator and slow poles (12, 13). Angular-momentum redistribution also drives a large-scale north–south meridional circulation (14–17). Long-term observations document the near-surface meridional flow. However, its depth dependence is much less clear, with different helioseismic techniques yielding different results (18–23).

Large-scale plasma motions must play a pivotal role in the stellar dynamo process. The latitudinal and radial shear provides a poloidal-to-toroidal conversion mechanism (i.e., the Ω effect) (24). Meridional circulation modulates the distribution of sunspots and may also establish the cycle timing (25–27). Helical flow generates a mean electromotive force (i.e., the α effect), which provides a toroidal-to-poloidal dynamo feedback (28–30). Any new information concerning interior fluid motions will produce valuable insight into the operation of the Sun's magnetic cycle.

Photospheric Convection. Several decades of observations have revealed much about solar surface convection (31, 32). Driven by fast radiative cooling, granulation dominates the radial motion at the solar surface. Roughly 1-Mm in horizontal size, granulation produces a strong power-spectrum peak at spherical harmonic degree ≈1,000 in radial Dopplergrams (33, 34). Significant power also exists at the ≈30 Mm supergranular scale, whose associated motions are mainly horizontal and best observed in limb Dopplergram spectra (35).

Photospheric power decreases monotonically for scales larger than supergranulation. From nonrotating intuition (36, 37), we might expect convective power to peak at ≈100 to 200-Mm (comparable with the convective-layer depth), rather than the ≈30-Mm supergranular scale. The results of refs. 38 and 39 indicate that deep-rooted fluid motions do persist on larger scales. Against expectations, however, these motions appear weak compared with the smaller-scale supergranular and granular flows. A great deal of theory and simulation work has attempted to solve the supergranulation problem, including direct formation

Significance

The entire Sun completes a full rotation in roughly 28 d. Within the outer 30% of the solar interior, turbulent thermal convection powers fluid outward. Rotation deflects the fluid and determines the morphology of eddies and large-scale shear. Such flows are the ultimate agents of astrophysical and planetary magnetic field generation, one of the most important open problems in all of science. Our results make theoretical predictions regarding the Sun's internal flow structure and rotational constraint. We predict tall and slender vortices persisting throughout much of the convection zone under the sway of strong rotation. We also clarify previous observational discrepancies and explain why such structures have been hard to reproduce in numerical simulations.

Author contributions: G.M.V. designed research; G.M.V. and K.J. performed research; G.M.V., K.J., and N.A.F. analyzed data; and G.M.V., K.J., and N.A.F. wrote the paper.

The authors declare no competing interest.

This article is a PNAS Direct Submission.

[1]To whom correspondence may be addressed. Email: geoffrey.vasil@sydney.edu.au.

This article contains supporting information online at https://www.pnas.org/lookup/suppl/doi:10.1073/pnas.2022518118/-/DCSupplemental.

Published July 29, 2021.

*Some geodynamo works refer to QG-MAC balance, which includes magnetism. In the Sun, magnetic energies are no greater than kinetic energy (i.e., MAC ∼ CIA). Conclusions drawn in this paper are insensitive to magnetism.

mechanisms (6, 37, 40–42). To date, no model self-consistently demonstrates how the supergranular scale might arise. We direct the reader to the recent review by Rincon et al. (43) for a thorough discussion of this topic. Our focus here is on the apparent lack of large-scale power as expected from nonrotating convection. We concur with results of past work (5, 44) that the supergranular scale results from suppression of power on large scales, rather than through preferential driving at that spatial scale.

Subphotospheric Convection. Local helioseismic techniques can probe subsurface convection directly [e.g., time distance (45), ring-diagram analysis (46), holography (47)]. Historically, these methods have largely been limited to ≈30-Mm depth and do not sample flow below the near-surface shear layer. As a result, numerical simulations play a substantial role in describing the dynamical balances in the deep convection zone.

Initially, nonlinear simulations of the full rotating solar convection zone seemed to reproduce the Sun's differential rotation profile. Those results suggested (as expected from nonrotating intuition) that convective power peaks at ≈100-Mm scales with ≈100-m/s flow-speed amplitudes (48, 49). Limitations of those results began to appear, however, with systematic magnetohydrodynamic studies in the ensuing decade. These studies found that only systems with ≈10× weaker flows or equivalently, those that rotated ≈10× faster, were able to produce coherent magnetic fields and periodic magnetic cycles in analogue to the Sun (50–55). Moreover, simulations with more extreme parameters and large-scale power can generate antisolar differential rotation, with slow equator and fast poles (14, 16, 17, 56–58). We also note that some recent observations suggest the Sun may lie near a boundary between these two basins in parameter space (59).

While most local helioseismic analyses focus on the near-surface shear layers, techniques have been developed to probe more deeply rooted flow structures, such as solar meridional circulation (60, 61). A notable puzzle arose following the deep-focusing time–distance analysis of Hanasoge et al. (1). This work placed a roughly 1-m/s upper limit on the ≈100-Mm-scale flow amplitudes at a depth ≈60 Mm. Subsequently, Greer et al. (2) sampled deeply enough to compare directly against the time–distance results at a depth of 30-Mm. Rather than no detection, this effort yielded measured flows that were 10 to 100× larger on those spatial scales. The discrepancies are still surprising even if they are measured at different depths. The disagreement between these results remains unresolved (11).

As an alternative to helioseismic measurement, the gyroscopic pumping effect (4) could, in principle, map the structure of deep convection. However, the technique requires accurate measurement of differential rotation and deep meridional circulation. Unfortunately, the current ambiguity in meridional circulation measurements makes this strategy presently impossible (18–23).

The Convective Conundrum. As a summary, we believe the following are all closely related questions.

- Where does supergranulation come from?
- Why are classic "giant cells" not observed?
- Why and exactly how do observations seem to contradict numerical models?

These questions all essentially ask the same thing: "Where is the large-scale convective power?" Some authors have recently studied possible direct formation mechanisms for supergranulation (6, 37, 40–42). In particular, recent work by Schumacher and coworkers (6, 37, 42) finds a continual amalgamation of convection on the largest scales admitted by the computational domain. Featherstone and Hindman (5) pointed out that rotational effects provide a natural explanation for the last two of these questions. Based on rotational effects, they suggested that the horizontal scale of deep convection must be no larger than the supergranular scale. They also estimated interior convective speeds significantly weaker than previously predicted. That work was numerical in nature, however. It did not describe the nature of deep-seated convection theoretically.

2. Analysis

Our goal is to estimate the dominant forces and their relative magnitudes. Our program is to manipulate the equations of motion into a form that exposes the principal dynamical balances as much as possible. We first define a general system of equations (under the anelastic approximation) that includes rotation (i.e., background profiles, momentum–mass–energy conservation, and radiation transport). We then isolate the place where rotational effects require a decision tree (i.e., the radiation flux balance). We define the tools of rotating theory (i.e., Rossby numbers [encoding the importance or lack of importance of rotational forces] and associated length scales). We proceed to answer the main question using an analysis of pressure or more specifically, the Bernoulli pressure function in our reformulation. The main question is what impact rotation has on the upper bounds for length scales and convective velocities. Finally, we highlight entropy, differential rotation, and thermal wind as consistency checks.

Background. In a coordinate frame with rotation rate, Ω around the $\hat{z}$ axis, the following is an exact reformulation of the fully compressible inviscid momentum equations

$$\partial_t u + (\nabla \times u + 2\Omega\,\hat{z}) \times u + \nabla\varpi \;=\; T\,\nabla s. \qquad [1]$$

The variable u is the local fluid velocity, T is temperature, and s is entropy per unit mass. Eq. **1** replaces the pressure, p, with the Bernoulli pressure function, ϖ, via the Second Law of Thermodynamics,

$$\frac{\mathrm{d}p}{\rho} \;=\; \mathrm{d}h - T\mathrm{d}s \quad \text{where} \quad \varpi \;\equiv\; \frac{|u|^2}{2} + h + \phi, \qquad [2]$$

where ρ is the mass density and h is the enthalpy per unit mass. Because the convection zone only contains 2% of the solar mass, $M_\odot$ (62), the gravitational potential $\phi \approx -GM_\odot/r$, where G is Newton's gravitational constant.

A well-mixed convection zone implies a well-defined adiabatic stratification (63), which varies only with the gravitational potential,

$$\mathrm{d}p_0 \;=\; -\rho_0 \mathrm{d}\phi, \quad \mathrm{d}h_0 \;=\; -\mathrm{d}\phi, \quad \mathrm{d}s_0 = 0. \qquad [3]$$

The exception happens in the upper ≈2%, where strong superadiabatic stratification drives flow close to the speed of sound.

Assuming an ideal gas law, $h_0 = c_p\,T_0 = \gamma p_0/\rho_0/(\gamma-1)$. The detailed specific heat depends on the ionization fraction and elemental abundances, which only become significant effects very near the solar surface. We assume constant values for c_p and $\gamma = 5/3$ (Table 1). Near the bottom of the convection zone, $T_0(R_{\text{c.z.}}) \approx 2.3 \times 10^6$ K. Near the surface, $T_0(R_\odot)/T_0(R_{\text{c.z.}}) \approx 10^{-3}$, which vanishes to a good approximation. The convection-zone radius $R_{\text{c.z.}} = R_\odot - H_{\text{c.z.}}$, where $H_{\text{c.z.}} \approx 200$ Mm is the convection-zone depth, and $R_\odot \approx 696$ Mm is the solar radius (Table 1). Therefore,

$$T_0(r) \;\approx\; \frac{\phi(R_\odot) - \phi(r)}{c_p} \;=\; T_0(R_{\text{c.z.}})\frac{R_{\text{c.z.}}}{H_{\text{c.z.}}}\frac{R_\odot - r}{r}. \qquad [4]$$

Table 1. Approximate parameters used for estimation calculations

Quantity	Symbol	Value	Unit
Solar mass	$M_\odot$	2.0×10^{30}	kg
Solar radius	$R_\odot$	6.9×10^{8}	m
Convection-zone radius	$R_{\text{c.z.}}$	0.71	$R_\odot$
Convection-zone depth	$H_{\text{c.z.}}$	0.29	$R_\odot$
Average rotation rate	Ω	2.6×10^{-6}	1/s
Total luminosity	$L_\odot$	3.8×10^{26}	W
Bottom temperature	$T_0(R_{\text{c.z.}})$	2.3×10^{6}	K
Bottom density	$\rho_0(R_{\text{c.z.}})$	210	kg/m^3
Bottom pressure	$p_0(R_{\text{c.z.}})$	6.7×10^{12}	Pa
Specific heat	c_p	3.4×10^{4}	J/kg/K
Adiabatic exponent	γ	5/3	

The convection-zone parameters come from Gough (62); the remaining parameters come from standard values.

For an adiabatic reference state,[†] $\rho_0(r) \propto T_0(r)^{3/2}$, $p_0(r) \propto T_0(r)^{5/2}$. The values at the base of the convection zone fix the constants of proportionality.

Momentum, Mass, and Energy. In the bulk of the convection zone, all thermodynamic variables fluctuate from their reference values by $\approx 10^{-6}$, which permits the anelastic approximation (64–66). Therefore,

$$\partial_t u + (\nabla \times u + 2\Omega\,\hat{z}) \times u + \nabla \varpi \;=\; T_0 \nabla s. \qquad \textbf{[5]}$$

The only difference between the fully compressible and anelastic momentum equation is the replacement $T \to T_0$. The anelastic approximation also implies nondivergent mass flux

$$\nabla \cdot (\rho_0 u) = 0. \qquad \textbf{[6]}$$

Energy transport closes the system:

$$\rho_0\, \partial_t \big(T_0 s + |u|^2/2 \big) + \nabla \cdot (\rho_0 \varpi u) = \nabla \cdot (K_0 \nabla T_0). \qquad \textbf{[7]}$$

Eq. **7** omits the diffusion of thermal fluctuations the same way Eq. **5** omits viscous dissipation. These effects are essential in a turbulent fluid but only become important for microscopic scales. We cannot, however, ignore the radiative diffusion of the background, which provides the heat that drives buoyancy (67).

Flux Balance. On average, energy transport requires

$$\langle \varpi u_r \rangle \;=\; \frac{1}{\rho_0} \left[\frac{L_\odot}{4\pi r^2} + K_0 \frac{dT_0}{dr} \right] \equiv\; F_0(r), \qquad \textbf{[8]}$$

where $L_\odot$ is the total solar luminosity. The angled bracket on the left-hand side of Eq. **8** represents an average over time and spherical surfaces, (θ, ϕ). We model the conductivity with Kramers' opacity (68) law,

$$K_0(r) \;=\; \frac{c_p L_\odot}{4\pi G M_\odot} \left[\frac{T_0(r)}{T_0(R_{\text{c.z.}})} \right]^{7/2}, \qquad \textbf{[9]}$$

which assumes $\rho_0^2 \propto T_0^3$. The two terms within the square brackets in Eq. **8** partially cancel because $K_0\, dT_0/dr < 0$. By definition, $F_0(R_{\text{c.z.}}) = 0$. We ignore the effect of convective overshooting, which would only produce tiny changes to the overall estimates. Eq. **8** is the foundation for all estimates; the right-hand side, $F_0(r)$, contains only known parameters.

[†]All quantities with a zero subscript denote adiabatic background reference states.

The quantity $F_0(r)$ represents a radiative "flux debt." Below the convection zone, radiative diffusion carries the entire luminosity. At some point near $R_{\text{c.z.}}$, the temperature gradient needed to carry the total flux becomes larger than the adiabatic gradient, and the system becomes unstable. Convection transports the remainder of the heat after the background relaxes to an almost adiabatic state. Eq. **8** carries dimensional units of velocity cubed. Standard mixing-length theory assumes $|u| \sim F_0^{1/3}$ (69). In slowly rotating situations, $F_0^{1/3}$ estimates the actual flow speed. More freedom exists in the rapidly rotating regime. Notably, $F_0(r)$ is not constant in radius, which implies the following two comments.

- No matter what, convective timescales are much slower than rotational timescales within some distance of the radiative zone.
- The important question is how far into the convection zone the rotation can dominate buoyancy.

To better understand these issues, we require a better understanding of the Bernoulli pressure function, ϖ.

Rossby Numbers, Length Scales, and Taylor–Proudman. The Rossby number measures the nondimensional ratio of convective-to-rotational acceleration. A common definition is the bulk Rossby number

$$\text{Ro}_{\text{b.}} \equiv \frac{|u|}{2\Omega\, H_\rho}, \qquad \textbf{[10]}$$

where $|u|$ represents a typical velocity amplitude and H_ρ is a density-scale height,

$$H_\rho \equiv \frac{c^2}{g} \;\approx\; (\gamma - 1) \frac{(R_\odot - r)\, r}{R_\odot}, \qquad \textbf{[11]}$$

where $c^2 = \gamma p_0/\rho_0$ and $g = GM_\odot/r^2$. Many references alternatively use the convection-zone depth $H_{\text{c.z.}}$ in place of the scale height (5) [i.e., $H_\rho(R_{\text{c.z.}})/H_{\text{c.z.}} \approx 0.46$]. Eq. **10** represents the ratio of relative-to-background vorticity assuming convective flows vary on a length scale comparable with H_ρ (or $H_{\text{c.z.}}$). Flows undoubtedly fluctuate over entire domain, but $\text{Ro}_{\text{b.}}$ overestimates rotational influence if the actual energy-containing scales are smaller than H_ρ.

Motivated by buoyancy considerations, the convective Rossby number is

$$\text{Ro}_{\text{c.}} \equiv \frac{\sqrt{\nabla T_0 \cdot \nabla \langle s \rangle}}{2\Omega}, \qquad \textbf{[12]}$$

where $\langle s \rangle$ represents mean entropy. This definition is equivalent to that used in the Boussinesq setting and defined in terms of the Rayleigh, Taylor, and Prandtl numbers, $\text{Ro}_{\text{c.}} \sim \sqrt{\text{Ra}/(\text{Pr Ta})}$ (70).

Assuming $\ell < H_\rho$ represents the actual (yet unknown) dynamical scale, we define an alternative dynamical Rossby number

$$\text{Ro}_{\text{d.}} \equiv \frac{|u|}{2\Omega\, \ell} \;\approx\; \frac{|\nabla \times u|}{2\Omega}. \qquad \textbf{[13]}$$

The dynamical Rossby number is the closest estimate of the actual ratio between local and background vorticity. All definitions relate to each other in some way and will coincide in the nonrotating regime.

The Taylor–Proudman theorem (71, 72) is an important constraint in systems where rotation dominates all other applied forces. The formal result comes from taking the curl of Eq. **5** and neglecting all effects other than rotation,

$$2\Omega\, \hat{z} \cdot \nabla u \;\approx\; 0. \qquad \textbf{[14]}$$

Strictly speaking, Eq. **14** is simply not true for convection. A generic system with boundaries cuts off the dynamics to fit

within the domain; hence, $|\hat{z}\cdot\nabla u|\sim|u|/H_{\rm c.z.}$. In a deep shell, $|\hat{z}\cdot\nabla u|\sim|u|/H_\rho$.

The more subtle view of the Taylor–Proudman constraint comes from considering the magnitude of the neglected terms. For $\mathrm{Ro_d}<1$, there is a substantial degree of anisotropy between the $\hat{z}$ and perpendicular directions,

$$\frac{\ell}{H_\rho}\approx\mathrm{Ro_d}\quad\Longleftrightarrow\quad\ell\approx\sqrt{\frac{|u|H_\rho}{2\Omega}}. \qquad [15]$$

Eq. **15** results from taking the curl of the momentum equations and balancing the resulting Coriolis terms against the nonlinear terms: that is,

$$2\Omega\,(\hat{z}\,\nabla\cdot u-\hat{z}\cdot\nabla u)\sim\nabla\times[(\nabla\times u)\times u], \qquad [16]$$

which is the CI part of the CIA balance. The curl eliminates leading-order geostrophic terms. Eq. **15** follows from estimating the left-hand side of Eq. **16** with $2\Omega|u|/H_\rho$ and the right-hand side with $|u|^2/\ell^2$.

Eq. **15** gives a direct link between flow speed and scale in a rapidly rotating system. Determining if this relation holds requires considering convective energy and momentum balances in detail.

This anisotropic picture of rotating convection has existed for many years in the Boussinesq convection community. The anisotropy principle is present in the linear-stability results in Chandrasekhar's famous book on hydrodynamic stability (73). Stevenson (74) expanded the understanding using linear theory, arriving at essentially the same scaling presented in Table 2. Ingersoll and Pollard (75) made a similar analysis applied to the interiors of planets. Sakai (76) observed the phenomena clearly in laboratory experiments. In a fully nonlinear and turbulent setting, Julien and coworkers (70, 77–81) have refined and promoted the principles of anisotropy and local Taylor–Proudman balance for strongly nonlinear flows since the mid-1990s; Aurnou et al. (10) has a current summary, including experimental evidence.

Stevenson (74) used incompressible linear theory to assess an optimal exponentially linear mode followed by an estimation of nonlinear saturation deduced from ideas leveraged from wave-mean theory. Julien et al. (79) independently reproduced the same theoretical scaling as obtained by Stevenson (74). This derivation used dimensional analysis and boundary-layer arguments for incompressible theory. Barker et al. (82) arrived at the same scaling yet again, in a modernized form. The approach used in the present manuscript is a force-balance approach intimately dependent on the processes that dictate the magnitude of the Bernoulli pressure. Detailed notions of rotational anisotropy have been slow to gain traction in the stratified stellar modeling community and astrophysics in general, although that has been changing in recent years (82–87). Overall, it seems that a consensus is forming surrounding the proper mechanical and thermal balances in rapidly rotating convection.

Table 2. Possible dynamical scaling in the large– and small–Rossby number regimes

Case	$\mathrm{Ro_d}$.	ℓ	$\lvert u\rvert$	$T_0\tilde{s}$	Condition
I	$\frac{F_0^{1/3}}{2\Omega H_\rho}$	H_ρ	$F_0^{1/3}$	$F_0^{2/3}$	$\mathrm{Ro_d}>1$
II	$\frac{F_0^{1/5}}{(2\Omega H_\rho)^{3/5}}$	$H_\rho\,\mathrm{Ro_d}$	$(F_0\mathrm{Ro_d})^{1/3}$	$\frac{F_0^{2/3}}{\mathrm{Ro_d}^{1/3}}$	$\mathrm{Ro_d}<1$

$\mathrm{Ro_d}$ represents the dynamical Rossby number (i.e., the ratio of local vorticity to rotation rate). $|u|$ and ℓ represent flow amplitude and length scale, respectively. The local timescale is $\tau=\ell/|u|$.

Pressure. If we know the size of ϖ in terms of ℓ and $|u|$, then Eqs. **8** and **15** give the characteristic magnitude of everything else. In fully compressible dynamics, the pressure (equivalently, ϖ) is a genuinely dynamical variable; it requires its own initial condition. In low–Mach number flows, the pressure becomes a Lagrange multiplier (66) that enforces the divergence-free condition by cancelling locally compressive terms. Finding an equation for ϖ requires multiplying Eq. **5** by ρ_0 and taking the divergence, which eliminates the time-evolution term and leaves an elliptic equation for ϖ. Because ϖ appears linearly, we can decompose the total Bernoulli pressure as a sum of three "partial pressures,"

$$\varpi\;\equiv\;\varpi_{\rm Kin.}+\varpi_{\rm Ther.}+\varpi_{\rm Rot.}. \qquad [17]$$

Each partial pressure responds to three separate sources

$$\nabla\cdot(\rho_0\nabla\varpi_{\rm Kin.})=\nabla\cdot(\rho_0\,u\times(\nabla\times u)), \qquad [18]$$
$$\nabla\cdot(\rho_0\nabla\varpi_{\rm Ther.})=\nabla\cdot(\rho_0\,T_0\nabla s), \qquad [19]$$
$$\nabla\cdot(\rho_0\nabla\varpi_{\rm Rot.})=\nabla\cdot(2\Omega\,\rho_0\,u\times\hat{z}). \qquad [20]$$

Solving Eqs. **18–20** in practice also requires appropriate boundary conditions of the same magnitude as the bulk sources.

We can estimate the size of each partial pressure from its source. First,

$$|\varpi_{\rm Kin.}|\;\sim\;|u|^2,\qquad|\varpi_{\rm Ther.}|\;\sim\;T_0|s|. \qquad [21]$$

At this point, the magnitude of $|s|$ is unknown, but we show later that it cannot dominate all other terms. If all three partial pressures are assumed roughly equal, then $|u|\sim F_0^{1/3}$. This has been the traditional assumption in mixing-length theory. However, it could also happen that the rotational (geostrophic) pressure dominates the kinetic pressure.

Eq. **20** differs from Eqs. **18** and **19** in that the left- and right-hand sides contain different numbers of derivatives. Geostrophy selects a length scale,

$$|\varpi_{\rm Rot.}|\;\sim\;2\Omega\,|u|\ell\;\sim\;\sqrt{2\Omega H_\rho\,|u|^3}. \qquad [22]$$

The crux of our argument is that the traditional mixing-length theory does not account for differences between $\varpi_{\rm Kin.}$ and $\varpi_{\rm Rot.}$ and the resulting implications. Altogether, we find two separate cases: CASE I in the slowly rotating scenario and CASE II in the rapidly rotating scenario. Table 2 has a summary.

Entropy. The magnitude of buoyancy variation poses a subtle question. The direct entropy evolution satisfies

$$\rho_0\,T_0\,(\partial_t s+u\cdot\nabla s)=\nabla\cdot(K_0\nabla T_0). \qquad [23]$$

The right-hand side radiative heating varies only in radius. The deviations from an adiabatic background, therefore, contain both mean and fluctuating parts: $s=\langle s\rangle(r)+\tilde{s}(r,\theta,\varphi)$.

Convection happens because large-scale entropy gradients become unstable to growing fluctuations. The instability saturates from turbulent transport counteracting the advection of the background. Specifically, $u\cdot\nabla\langle s\rangle\sim u\cdot\nabla\tilde{s}$, or

$$\ell\;\langle s-s_0\rangle\;\sim\;H_\rho\;\tilde{s}, \qquad [24]$$

where $\langle s_0\rangle$ represents the global mean adiabat. An estimate for $\tilde{s}$ follows from the curl of the momentum equations,

$$\nabla\times[(\nabla\times u)\times u]\;\sim\;\nabla T_0\times\nabla\tilde{s}, \qquad [25]$$

which is the IA part of CIA balance. Therefore,

$$T_0\,\tilde{s} \sim \frac{|u|^2}{\mathrm{Ro_{d.}}}, \qquad T_0\,\langle s - s_0\rangle \sim \frac{|u|^2}{\mathrm{Ro_{d.}^2}}. \qquad [26]$$

Putting everything together, in the rapidly rotating regime (10),

$$\mathrm{Ro_{c.}} \sim \frac{\mathrm{Ro_{b.}}}{\mathrm{Ro_{d.}}} \sim \mathrm{Ro_{d.}}. \qquad [27]$$

With all the theoretical elements in place, we apply our analysis to the solar convection zone.

Summary of Closed Balances. We give a summary of the minimal chain of reasoning needed to arrive at the results outlined in Table 2. CASES I and II denote nonrotating and rapidly rotating regimes, respectively:

$$\text{CASE I and II:} \quad \varpi|u| \sim F_0 \qquad [28]$$

$$\begin{aligned} &\text{CASE I:} \quad \varpi \sim |u|^2 \quad \ell \sim H_\rho \\ &\text{CASE II:} \quad \tfrac{\varpi}{\ell} \sim 2\Omega|u| \quad \tfrac{\ell}{H_\rho} \sim \tfrac{|u|}{2\Omega\ell}. \end{aligned} \qquad [29]$$

Assuming rapid rotation, flux transport, geostrophy, and Taylor–Proudman determine the length scale and flow amplitude. The Bernoulli pressure acts as the crucial mediator. We can also rephrase these balances in the nondimensional language of rotating Rayleigh–Bénard convection theory. Defining the Ekman, Rayleigh, and Prandtl numbers,

$$\mathrm{Ek} = \frac{\nu}{2\Omega {H_\rho}^2}, \quad \mathrm{Ra} = \frac{\nabla T_0 \cdot \nabla\langle s\rangle {H_\rho}^4}{\nu\kappa}, \quad \mathrm{Pr} = \frac{\nu}{\kappa}, \qquad [30]$$

where ν, κ represent the viscous and thermal diffusivities, respectively. The linear theory of onset predicts that $\ell/H_\rho \sim \mathrm{Ek}^{1/3}$ and $\mathrm{Ra} \sim \mathrm{Ek}^{-4/3}$. In general, sufficiently above onset

$$\ell/H_\rho \sim \mathrm{Ek}^{1/3}\,(\mathrm{Ra}\,\mathrm{Ek}^{4/3})^\alpha\,\mathrm{Pr}^\beta. \qquad [31]$$

Our inviscid balances correspond to $\alpha = 1/2$, $\beta = -1/2$. Some recent works (7, 8) find $\ell/H_\rho \sim \Omega^{-1/3}$ in high-resolution numerical simulations. The only way for this to happen is if $\alpha = 0$. Independence of the criticality suggests that even the best simulations are still close to onset. The Reynolds number depends directly on the criticality, $\mathrm{Re} \sim (\mathrm{Ra}\,\mathrm{Ek}^{4/3})^{3\alpha}\,\mathrm{Pr}^{3\beta}$. For example, the most extreme parameters of figure 1C in ref. 8 show only a twofold difference between the measured inertial and viscous forces.

3. Results

Table 1 summarizes the parameters used to estimate the Rossby number, convective velocities, and length scales.

Fig. 1*A* shows Rossby number estimates as a function of depth. If we assume the traditional CASE I scenario, we find $\mathrm{Ro_{d.}} < 1$ for $r/R_\odot \lesssim 0.93$. This is a contradiction because CASE I presumes no rotational influence, and hence, CASE II must apply instead. While $\mathrm{Ro_{d.}}$ is not asymptotically small, it is less the unity for most of the convection zone and is less than 0.5 for the bottom half. Fig. 1*B* shows flow amplitude. The flow speed is only slightly less in the rotating regime than the nonrotating equivalent. A weak power of the Rossby number distinguishes between CASES I and II.

The dynamical length scale is the most dramatic effect of rapid rotation. Fig. 2 shows a consistent size for most of the convection zone, which is also much smaller than the bulk depth,

$$\ell \approx 0.15 H_{\mathrm{c.z.}} \approx 30\mathrm{-Mm}. \qquad [32]$$

This number happens to coincide with the characteristic length scale of supergranulation, with spherical harmonic degree ≈ 120-150.

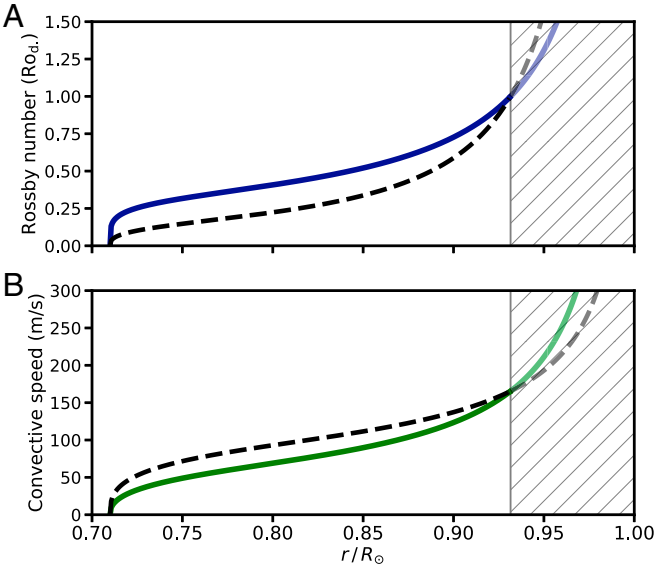

Fig. 1. (*A*) The estimated dynamical Rossby number as a function of depth. (*B*) The estimated convective flow speed estimates as a function of depth. In both panels, the solid curves represent the rapidly rotating regime (CASE II). The dashed lines show the slowly rotating counterfactual (CASE I). Both $\mathrm{Ro_{d.}}$ estimates are less than unity for much of the convection zone; hence, rotating assumptions apply. The shaded regions above $r/R_\odot \approx 0.93$ mark where rotational effects are subdominant. Several other effects become important in the outer layers.

Effects of Geometry. A question remains how the misalignment of gravity and the rotation axis affects the estimates. Several studies investigated the dependence on the local latitude in Cartesian domains (86, 88–91). No results seem definitive, and much of the effort is still ongoing. Achieving rotational constraint at solar parameters requires a domain large enough to experience the variation of background forces. A sizable energy-containing eddy near the equator will feel off-equator effects.

Table 2 depends on H_ρ, which entered the analysis by assuming $\hat{z}\cdot\nabla \sim 1/H_\rho \lesssim 1/H_{\mathrm{c.z.}}$. Variation along the rotation axis is the important overall reference length scale. The poles pose no challenge, where $\hat{r} \approx \hat{z}$. However, starting from the equator, the distance from $r = R_{\mathrm{c.z.}}$ to $r = R_\odot$ in the $\hat{z}$ direction is

$$H_z = H_{\mathrm{c.z.}}\sqrt{2R_{\mathrm{c.z.}}/H_{\mathrm{c.z.}} + 1} \approx 5H_\rho. \qquad [33]$$

We, therefore, expect at low latitudes modest increases to the true length scale appearing in Table 2, $\ell \propto H_z^{2/5} \approx 1.9 {H_\rho}^{2/5}$. However, $\mathrm{Ro_{d.}} \propto H_z^{-3/5} \approx 0.4 {H_\rho}^{-3/5}$, and $|u| \propto H_z^{-1/5} \approx 0.7 {H_\rho}^{-1/5}$. Moreover, these estimates are the extreme case. Therefore, near the equator, we might expect Fig. 2 to show a slight increase in scale (perhaps up to ≈50-60 Mm for $r \approx R_{\mathrm{c.z.}}$), but this would be accompanied by slower flows and additional rotational constraint.

Differential Rotation. Helioseismology provides a few additional checks on the overall rectitude of our estimates. Even with some differences, convection and shear provide proxies for one another (87). Helioseismology, therefore, presents a consistency check for some of our estimates.

As a function of radius, r, and colatitude, θ, the local rotation rate $\Omega(r,\theta)$ implies an angular inertial-frame bulk flow $u = r\sin\theta\,\Omega\,\hat{\varphi}$, which implies a total vorticity,

$$\nabla\times(r\sin\theta\,\Omega\,\hat{\varphi}) = 2\Omega\,\hat{z} + r\sin\theta\,\nabla\Omega\times\hat{\varphi}. \qquad [34]$$

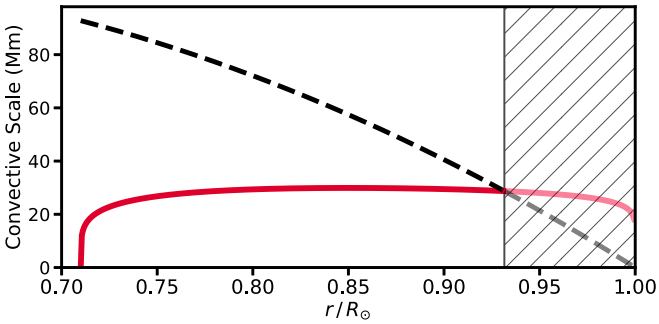

Fig. 2. The convective length-scale estimate as a function of depth in the solar convection zone. The solid red curve shows the estimate under the rapidly rotating assumption (CASE II). The dashed line shows the $H_\rho(r)$ profile from Eq. **11** (CASE I). The shaded region above $r/R_\odot \approx 0.93$ marks where rotation is subdominant (i.e., a depth ≈50 Mm). The rotationally constrained length scale stays consistently ≈30-Mm and is the length scale realized below $r/R_\odot \approx 0.93$. The density-scale height becomes the dominant length scale only in the near-surface regions.

Assuming the differential rotation is strongly coupled to the dynamics,

$$\mathrm{Ro_{d.}} \approx \frac{r\sin\theta|\nabla\Omega|}{2\Omega}. \qquad [35]$$

Fig. 3 shows the local Rossby number of the differential rotation as a function of latitude and depth in the convection zone. The data come from the local rotation rate in Larson and Schou (92).[‡] We compute the gradient of $\Omega(r,\theta)$ with a fourth-order finite difference derivative. A few pertinent observations are in order. The Rossby number is never more than 0.4 for $r/R_\odot < 0.95$. The tachocline ($0.65 < r/R_\odot < 0.75$) dominates the picture in the deep interior. The radiative zone is almost in solid-body rotation, and therefore, the shear Rossby number nearly vanishes. Above $r/R_\odot \approx 0.95$, the rapid increase of the Rossby number indicates the start of the near-surface shear layer, which is poorly understood. However, for much of the bulk convection zone, the differential rotation Rossby number hovers consistently around ≈0.1.

Also intriguing, the half-width of the tachocline bump is ≈ 35-Mm, which is consistent with the ≈30-Mm estimate for the convection. If convection maintains the tachocline, it seems reasonable that their sizes should match. We are aware that the resolution of helioseismology degrades with depth and that tachocline widths are upper bounds on the actual thickness. Even so, the data from helioseismology accord with simple dynamical estimates.

Thermal Wind. The above picture of differential rotation is consistent with the large-scale thermal-wind model of Balbus et al. (93). The above scaling allows a significant balance between

$$r^2\sin(\theta)\,\partial_z\Omega^2 \;\approx\; -T_0'(r)\,\partial_\theta\tilde{s}. \qquad [36]$$

Thermal wind results from taking the curl of the momentum equation and balancing global vortex stretching with baroclinic production. The balance should exist in any thermally driven rapidly rotating system; it results from neglecting convective inertia and dissipation. There has been some discussion in the literature regarding the precise degree of global thermal-wind balance in the convection zone (94). It is becoming clear how sensitive differential rotation can be to large-scale thermal gradients (95). Eq. **36** does not necessarily give the exact large-scale entropy profile (e.g., due to possible subdominant Reynolds and Maxwell stress corrections), but it gives a good indication and provides a consistency check.

Fig. 4 shows a solution to Eq. **36**. We integrate the right-hand side over θ using the trapezoidal rule. As Balbus et al. (93) pointed out, we can freely add any radial function to the solution. We set the integration constant by $\int_0^\pi \tilde{s}(r,\theta)\sin(\theta)\mathrm{d}\theta = 0$. The entropy state needed to maintain differential rotation is roughly the same that is needed to drive rotationally constrained turbulent convection. From Eq. **26**, we estimate $T_0\tilde{s} \sim (2\Omega H_\rho F_0^3)^{1/5}$, but this should be interpreted carefully. By definition, the thermal-wind entropy contains no mean radial gradient. The convective flux debt contains only a radial profile and vanishes at the base of the convection zone (also by definition). Nevertheless, different entropy profiles match in a characteristic sense. Fig. 5 shows the latitudinal rms thermal wind as a function of radius along with the radial convective estimates. The thermal-wind profile does not distinguish between rotating vs. nonrotating hypotheses. The two predictions differ by a low power of the Rossby number. Nevertheless, the independently measured differential rotation provides a consistency check on theory derived from flux-balance considerations. Also noteworthy, Fig. 4 suggest the thermal-wind entropy is better mixed near the equator than near the poles.

4. Conclusions

Based on well-understood physics, we furnish a detailed estimate of the degree of rotational constraint in the solar interior.

We summarize our assumptions as follows.

- Solar convection comprises negligibly viscous convective fluctuations around a nearly adiabatic hydrostatic background.
- Convective turbulence transports a radiative flux debt (i.e., the part of the solar luminosity that an adiabatic temperature gradient cannot carry).
- The definition of "rapid rotation" is equivalent to leading-order balance between Coriolis and pressure forces (QG), followed by a joint triple balance between inertia, buoyancy, and the nondivergent component of Coriolis deflections (CIA).

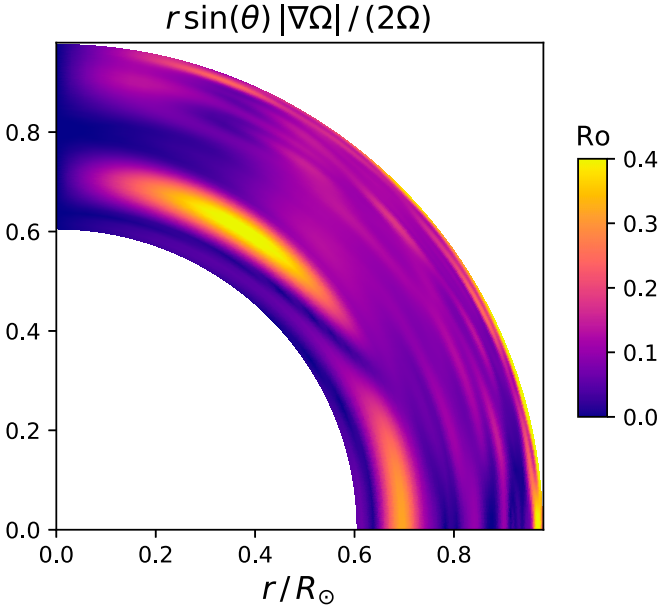

Fig. 3. The local Rossby number computed from helioseismic-inferred profile $\Omega(r,\theta)$ in the convection zone. We use a fourth-order finite difference to compute the gradient from the raw rotation rate data, which are found in the electronic supplementary material from Larson and Schou (92).

[‡]The data are from the electronic supplementary material for the article "Global-mode analysis of full-disk data from the Michelson doppler imager and helioseismic and magnetic imager" (93).

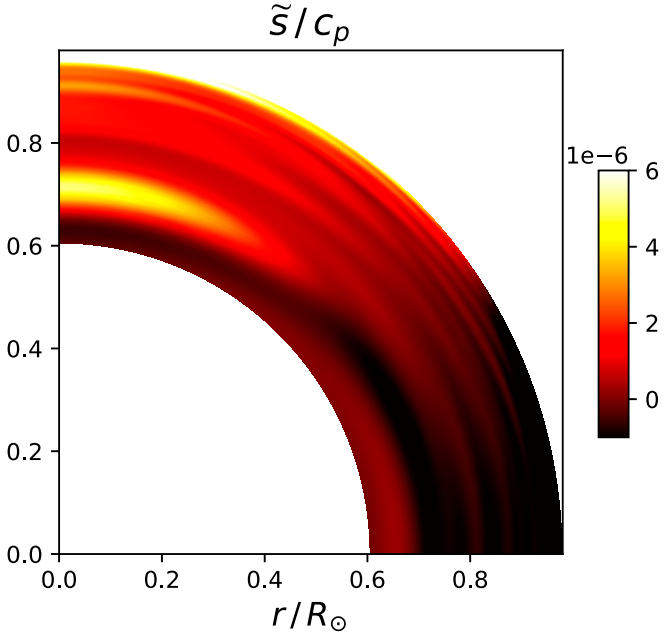

Fig. 4. The local thermal-wind entropy profile computed from helioseismic-inferred profile $\Omega(r, \theta)$ in the convection zone. We use a fourth-order finite difference to compute $\partial_z = \cos\theta\partial_r - r^{-1}\sin\theta\partial_\theta$ and a trapezoidal rule to integrate over θ. The data are found in the electronic supplementary material from Larson and Schou (92).

- Magnetic energies should be roughly similar to kinetic energies. At most, we expect $|B| \lesssim \sqrt{\mu_0\rho_0}|u|$, which does not alter any of our conclusions.

We summarize our results as follows.

- The solar convection zone is rotationally constrained roughly everywhere below the near-surface shear layer.
- The flow amplitudes in the rotating regime are similar to what would exist in the absence of rotation.
- Rotation noticeably reduces the dynamical length scale. We predict ≈30-Mm robustly throughout the convection zone.
- The strongest flow gradients are perpendicular to the rotation axis, with scales $\sim H_\rho \approx$100 to 200-Mm variation in the $\hat{z}$ direction.
- Individual deep convective structures should persist for multiple rotation periods.
- Solar differential rotation is itself strongly rotationally influenced and indicative of the above conclusions.
- Both the equator and poles experience strong rotational influence. Moreover, there should exist significant differences between the flow signatures observable in different regions.

The 30-Mm prediction is intriguing for several reasons. First, the scale matches the observed size of surface supergranulation. While it is tempting to suggest supergranulation is the surface manifestation of deep convection, we do not believe the situation is altogether this simple. While the spatial scales do match, the timescale of supergranulation is fast compared with rotation (i.e., ≈1 d vs. ≈1 mo). It also happens that $\mathrm{Ro_d} \approx 1$ at $r/R_\odot \approx 0.93$, which is ≈50 Mm below the surface. While they may not be literally the same phenomena, a spatial matching means that the different phenomena can interact in interesting ways. We hope future studies will clarify the connections between anisotropic deep convection, supergranulation, and the near-surface shear layer. All three processes surely interact in unforeseen ways with magnetism (e.g., refs. 96 and 97).

We also believe our estimates resolve several past questions regarding observations and simulations. First, we believe the observation of Hanasoge et al. (1) finds anomalously low signals because of a scale effect, rather than a genuinely small flow. We believe our estimates are inconsistent with the results from ref. 2. The new results of Hanasoge et al. (3) also appear to imply this. It is not clear what kind of signal should exist at ≈200-Mm scales, given a true peak of power at ≈30-Mm scales. However, a direct and local inverse cascade should be weak. We anticipate at least an order of magnitude reduction. Specifically, an inverse cascade should transfer energy to barotropic differential rotation, not to larger convective motions (80, 98–102).

Our estimates also address numerous stellar convection simulations carried out in recent decades. Any simulation with spherical harmonic degree less than ≈1,000 is unlikely to resolve a spectrum of low–Rossby and large–Reynolds number convection (103). It is not enough to only just resolve 30-Mm structures. These features must also not dissipate viscously or thermally, as they surely do not in the real Sun. We believe that the simulations of Featherstone and Hindman (5) represent the first spherical simulations convincingly in this challenging computational regime. As computational tools improve (104, 105), studies of this type are becoming increasingly more feasible (e.g., ref. 106). Moreover, it is possible that after the rotational length scales are safely captured in a low-friction regime, there may be diminishing returns from continued resolution increases.

How can these predictions be tested against observations? The expectation of vorticity parallel to the rotation axis offers a promising possibility. Unfortunately, helioseismic techniques are relatively insensitive to radial flow and are confined to regions within 60° of disk center. Helioseismically measuring vorticity parallel to the rotational axis is quite difficult from the ecliptic plane. Techniques based on tracking supergranules fare a bit better away from disk center, and recent results appear to indicate the presence of large-scale vortical, cellular motions in the Sun's polar regions (39). Even better, observations from a polar vantage could use multiple techniques to analyze vorticity. Such high-latitude measurement are, therefore, becoming more crucial if theory and observations are to meet.

Finally, we point out that the Sun rotated faster earlier in its history. It was also smaller and less luminous. All of these effects will surely produce an interesting interplay in the dynamical Rossby number, dominant length scales, and hence, magnetic

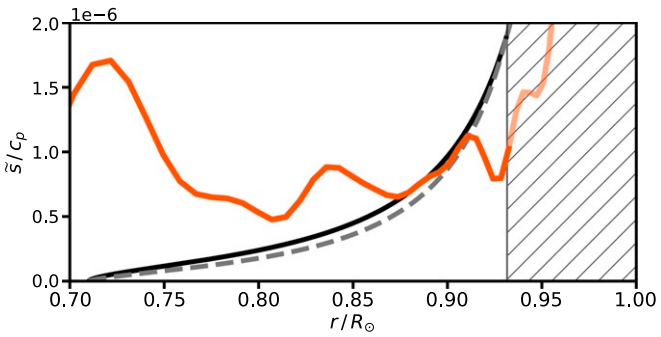

Fig. 5. Radial entropy profiles. The orange curve is the θ rms of the two-dimensional profile from Fig. 4. The black curve is the convective estimate regime based on the flux debt; $(2\Omega H_\rho F_0^3)^{1/5}/h_0$ with background enthalpy $h_0 = c_p T_0$. The dashed curve shows the estimate based on nonrotating theory, $F_0^{2/3}/h_0$. By magnitude, all three of these profiles are consistent. Distinguishing rotating vs. nonrotating theories lies with other quantities, particularly the convective length scale.

field generation. However, global magnetism is the cause of rotational spin down. The nature of magnetic breaking in stars is far from settled (107). We hope our estimates motivate future studies in rotating and magnetized systems outside the present-day Sun.

Data Availability. All study data are included in the article and/or supporting information. Additionally, previously published data were used for this work (92).

ACKNOWLEDGMENTS. We thank Ben Brown for locating the differential rotation data used in this work and for helpful comments on manuscript and Brad Hindman for helpful conversations. We also thank Jon Aurnou for detailed comments, especially on *SI Appendix*. We thank one of the anonymous referees for suggestions that greatly improved the manuscript. G.M.V. thanks Eliot Quataert for hosting in Berkeley in 2015, where much of this work was done, and for helpful comments in the early stages. K.J. acknowledges support from NASA Grant 80NSSC17K0008 and NSF Grant DMS-2009319. N.A.F. acknowledges support from NASA Grants 80NSSC17K0008 and 80NSSC20K0193.

1. S. M. Hanasoge, T. L. Duvall Jr., K. R. Sreenivasan, Anomalously weak solar convection. *Proc. Natl. Acad. Sci. U.S.A.* **109**, 11928–11932 (2012).
2. B. J. Greer, B. W. Hindman, J. Toomre, Helioseismic imaging of supergranulation throughout the sun's near-surface shear layer. *Astrophys. J.* **824**, 128 (2016).
3. S. M. Hanasoge, H. Hotta, K. R. Sreenivasan, Turbulence in the Sun is suppressed on large scales and confined to equatorial regions. *Sci. Adv.* **6**, eaba9639 (2020).
4. M. S. Miesch, N. A. Featherstone, M. Rempel, R. Trampedach, On the amplitude of convective velocities in the deep solar interior. *Astrophys. J.* **757**, 128 (2012).
5. N. A. Featherstone, B. W. Hindman, The emergence of solar supergranulation as a natural consequence of rotationally constrained interior convection. *Astrophys. J.* **830**, L15 (2016).
6. J. Schumacher, K. R. Sreenivasan, Colloquium: Unusual dynamics of convection in the sun. *Rev. Mod. Phys.* **92**, 041001 (2020).
7. N. Gillet, C. A. Jones, The quasi-geostrophic model for rapidly rotating spherical convection outside the tangent cylinder. *J. Fluid Mech.* **554**, 343 (2006).
8. R. K. Yadav, T. Gastine, U. R. Christensen, S. J. Wolk, K. Poppenhaeger, Approaching a realistic force balance in geodynamo simulations. *Proc. Natl. Acad. Sci. U.S.A.* **113**, 12065–12070 (2016).
9. T. Schwaiger, T. Gastine, J. Aubert, Force balance in numerical geodynamo simulations: A systematic study. *Geophys. J. Int.* **219**, S101–S114 (2019).
10. J. M. Aurnou, S. Horn, K. Julien, Connections between nonrotating, slowly rotating, and rapidly rotating turbulent convection transport scalings. *Phys. Rev. Res.* **2**, 043115 (2020).
11. K. Nagashima, A. C. Birch, J. Schou, B. W. Hindman, L. Gizon, An improved multi-ridge fitting method for ring-diagram helioseismic analysis. *Astron. Astrophys.* **633**, A109 (2020).
12. R. Howe, Solar interior rotation and its variation. *Living Rev. Sol. Phys.* **6**, 1 (2009).
13. M. J. Thompson, J. Christensen-Dalsgaard, M. S. Miesch, J. Toomre, The internal rotation of the sun. *Annu. Rev. Astron. Astrophys.* **41**, 599–643 (2003).
14. T. Gastine, R. K. Yadav, J. Morin, A. Reiners, J. Wicht, From solar-like to antisolar differential rotation in cool stars. *Mon. Not. R. Astron. Soc. Lett.* **438**, L76–L80 (2013).
15. T. Gastine, M. Heimpel, J. Wicht, Zonal flow scaling in rapidly-rotating compressible convection. *Phys. Earth Planet. Inter.* **232**, 36–50 (2014).
16. G. Guerrero, P. K. Smolarkiewicz, A. G. Kosovichev, N. N. Mansour, Differential rotation in solar-like stars from global simulations. *Astrophys. J.* **779**, 176 (2013).
17. N. A. Featherstone, M. S. Miesch, Meridional circulation in solar and stellar convection zones. *Astrophys. J.* **804**, 67 (2015).
18. D. H. Hathaway, D. Nandy, R. M. Wilson, E. J. Reichmann, Evidence that a deep meridional flow sets the sunspot cycle period. *Astrophys. J.* **589**, 665–670 (2003).
19. D. H. Hathaway, L. Rightmire, Variations in the Sun's meridional flow over a solar cycle. *Science* **327**, 1350–1352 (2010).
20. R. K. Ulrich, Solar meridional circulation from Doppler shifts of the Fe I line at 5250 Å as measured by the 150-foot solar tower telescope at the Mt. Wilson observatory. *Astrophys. J.* **725**, 658–669 (2010).
21. S. Kholikov, A. Serebryanskiy, J. Jackiewicz, Meridional flow in the solar convection zone. I. Measurements from GONG data. *Astrophys. J.* **784**, 145 (2014).
22. J. Jackiewicz, A. Serebryanskiy, S. Kholikov, Meridional flow in the solar convection zone. II. Helioseismic inversions of GONG data. *Astrophys. J.* **805**, 133 (2015).
23. L. Gizon *et al*., Meridional flow in the Sun's convection zone is a single cell in each hemisphere. *Science* **368**, 1469–1472 (2020).
24. M. Ossendrijver, The solar dynamo. *Astron. Astrophys. Rev.* **11**, 287–367 (2003).
25. M. Dikpati, P. Charbonneau, A Babcock-Leighton flux transport dynamo with solar-like differential rotation. *Astrophys. J.* **518**, 508–520 (1999).
26. A. R. Yeates, D. Nandy, D. H. Mackay, Exploring the physical basis of solar cycle predictions: Flux transport dynamics and persistence of memory in advection-versus diffusion-dominated solar convection zones. *Astrophys. J.* **673**, 544–556 (2008).
27. A. Muñoz-Jaramillo, D. Nandy, P. C. H. Martens, Helioseismic data inclusion in solar dynamo models. *Astrophys. J.* **698**, 461–478 (2009).
28. K. H. Moffatt, *The Generation of Magnetic Fields in Electrically Conducting Fluids* (Cambridge University Press, 1978).
29. P. Olson, U. Christensen, G. A. Glatzmaier, Numerical modeling of the geodynamo: Mechanisms of field generation and equilibration. *J. Geophys. Res. Solid Earth* **104**, 10383–10404 (1999).
30. P. A. Davidson, *An Introduction to Magnetohydrodynamics* (Cambridge University Press, 2001).
31. A. B. Hart, Motions in the sun at the photospheric level. VI. Large-scale motions in the equatorial region. *Mon. Not. R. Astron. Soc.* **116**, 38–55 (1956).
32. R. B. Leighton, R. W. Noyes, G. W. Simon, Velocity fields in the solar atmosphere. I. Preliminary report. *Astrophys. J.* **135**, 474 (1962).
33. D. Hathaway *et al*., The photospheric convection spectrum. *Sol. Phys.* **193**, 299–312 (2000).
34. D. H. Hathaway, T. Teil, A. A. Norton, I. Kitiashvili, The sun's photospheric convection spectrum. *Astrophys. J.* **811**, 105 (2015).
35. J. K. Lawrence, A. C. Cadavid, A. A. Ruzmaikin, Characteristic scales of photospheric flows and their magnetic and temperature markers. *Astrophys. J.* **513**, 506–515 (1999).
36. G. Ahlers, S. Grossmann, D. Lohse, Heat transfer and large scale dynamics in turbulent Rayleigh-Bénard convection. *Rev. Mod. Phys.* **81**, 503–537 (2009).
37. A. Pandey, J. D. Scheel, J. Schumacher, Turbulent superstructures in Rayleigh-Bénard convection. *Nat. Commun.* **9**, 2118 (2018).
38. D. H. Hathaway, L. Upton, O. Colegrove, Giant convection cells found on the Sun. *Science* **342**, 1217–1219 (2013).
39. D. H. Hathaway, L. A. Upton, Hydrodynamic properties of the Sun's giant cellular flows. *Astrophys. J.* **908**, 160 (2021).
40. J. F. Cossette, M. P. Rast, Supergranulation as the largest buoyantly driven convective scale of the sun. *Astrophys. J.* **829**, L17 (2016).
41. M. Kessar, D. W. Hughes, E. Kersalé, K. A. Mizerski, S. M. Tobias, Scale selection in the stratified convection of the solar photosphere. *Astrophys. J.* **874**, 103 (2019).
42. P. P. Vieweg, J. D. Scheel, J. Schumacher, Supergranule aggregation for constant heat flux-driven turbulent convection. *Phys. Rev. Res.* **3**, 013231 (2021).
43. F. Rincon, T. Roudier, A. A. Schekochihin, M. Rieutord, Supergranulation and multiscale flows in the solar photosphere. *Astron. Astrophys.* **599**, A69 (2017).
44. J. W. Lord, R. H. Cameron, M. P. Rast, M. Rempel, T. Roudier, The role of subsurface flows in solar surface convection: Modeling the spectrum of supergranular and larger scale flows. *Astrophys. J.* **793**, 24 (2014).
45. T. L. Duvall, S. M. Jeffferies, J. W. Harvey, M. A. Pomerantz, Time-distance helioseismology. *Nature* **362**, 430–432 (1993).
46. S. Basu, H. M. Antia, S. C. Tripathy, Ring diagram analysis of near-surface flows in the sun. *Astrophys. J.* **512**, 458–470 (1999).
47. C. Lindsey, D. C. Braun, Helioseismic holography. *Astrophys. J.* **485**, 895–903 (1997).
48. A. S. Brun, J. Toomre, Turbulent convection under the influence of rotation: Sustaining a strong differential rotation. *Astrophys. J.* **570**, 865–885 (2002).
49. M. S. Miesch, A. S. Brun, J. Toomre, Solar differential rotation influenced by latitudinal entropy variations in the tachocline. *Astrophys. J.* **641**, 618–625 (2006).
50. M. Ghizaru, P. Charbonneau, P. K. Smolarkiewicz, Magnetic cycles in global large-eddy simulations of solar convection. *Astrophys. J. Lett.* **715**, L133–L137 (2010).
51. É. Racine, P. Charbonneau, M. Ghizaru, A. Bouchat, P. K. Smolarkiewicz, On the mode of dynamo action in a global large-eddy simulation of solar convection. *Astrophys. J.* **735**, 46 (2011).
52. B. P. Brown, M. S. Miesch, M. K. Browning, A. S. Brun, J. Toomre, Magnetic cycles in a convective dynamo simulation of a young solar-type star. *Astrophys. J.* **731**, 69 (2011).
53. P. J. Käpylä, M. J. Mantere, A Brand enburg, cyclic magnetic activity due to turbulent convection in spherical wedge geometry. *Astrophys. J. Lett.* **755**, L22 (2012).
54. J. Warnecke, P. J. Käpylä, M. J. Käpylä, A. Brandenburg, On the cause of solar-like equatorward migration in global convective dynamo simulations. *Astrophys. J. Lett.* **796**, L12 (2014).
55. N. J. Nelson, B. P. Brown, A. S. Brun, M. S. Miesch, J. Toomre, Buoyant magnetic loops generated by global convective dynamo action. *Sol. Phys.* **289**, 441–458 (2014).
56. T. Gastine, J. Wicht, J. M. Aurnou, Zonal flow regimes in rotating anelastic spherical shells: An application to giant planets. *Icarus* **225**, 156–172 (2013).
57. P. J. Käpylä, M. J. Käpylä, A Brand enburg, Confirmation of bistable stellar differential rotation profiles. *Astron. Astrophys.* **570**, A43 (2014).
58. A. S. Brun, M. K. Browning, Magnetism, dynamo action and the solar-stellar connection. *Living Rev. Sol. Phys.* **14**, 4 (2017).
59. T. S. Metcalfe, R. Egeland, J. van Saders, Stellar evidence that the solar dynamo may be in transition. *Astrophys. J.* **826**, L2 (2016).
60. T. Hartlep, J. Zhao, A. G. Kosovichev, N. N. Mansour, Solar wave-field simulation for testing prospects of helioseismic measurements of deep meridional flows. *Astrophys. J.* **762**, 132 (2013).
61. J. Zhao, R. S. Bogart, A. G. Kosovichev, T. L. Duvall, T. Hartlep, Detection of equatorward meridional flow and evidence of double-cell meridional circulation inside the sun. *Astrophys. J.* **774**, L29 (2013).
62. D. Gough, "An introduction to the solar tachocline" in *The Solar Tachocline*, D. W. Hughes, R. Rosner, N. O. Weiss, Eds. (Cambridge University Press, 2007), pp. 3–30.
63. J. Christensen-Dalsgaard, Helioseismology. *Rev. Mod. Phys.* **74**, 1073–1129 (2002).
64. D. O. Gough, The anelastic approximation for thermal convection. *J. Atmos. Sci.* **26**, 448–456 (1969).
65. B. P. Brown, G. M. Vasil, E. G. Zweibel, Energy conservation and gravity waves in sound-proof treatments of stellar interiors. Part I. Anelastic approximations. *Astrophys. J.* **756**, 109 (2012).
66. G. M. Vasil, D. Lecoanet, B. P. Brown, T. S. Wood, E. G. Zweibel, Energy conservation and gravity waves in sound-proof treatments of stellar interiors. Part II. Lagrangian-constrained analysis. *Astrophys. J.* **773**, 169 (2013).

67. S. Lepot, S. Aumaître, B. Gallet, Radiative heating achieves the ultimate regime of thermal convection. *Proc. Natl. Acad. Sci. U.S.A.* **115**, 8937–8941 (2018).
68. P. J. Käpylä, M. Viviani, M. J. Käpylä, A. Brandenburg, F. Spada, Effects of a subadiabatic layer on convection and dynamos in spherical wedge simulations. *Geophys. Astrophys. Fluid Dyn.* **113**, 149–183 (2019).
69. E. Böhm-Vitense, Uber wasserstoffkonvektions-zone in sternen und leuchtkra "fte."*Z. Astrophys.* **46**, 108–143 (1958).
70. K. Julien, S. Legg, J. Mcwilliams, J. Werne, Rapidly rotating turbulent Rayleigh-Bénard convection. *J. Fluid Mech.* **322**, 243–273 (1996).
71. J. Proudman, On the motion of solids in a liquid possessing vorticity. *Proc. R. Soc. Lond., A Contain. Pap. Math. Phys. Character* **92**, 408–424 (1916).
72. G. I. Taylor, Motion of solids in fluids when the flow is not irrotational. *Proc. R. Soc. Lond., A Contain. Pap. Math. Phys. Character* **93**, 99–113 (1917).
73. S. Chandrasekhar, *Hydrodynamic and Hydromagnetic Stability* (Oxford University Press, 1961).
74. D. J. Stevenson, Turbulent thermal convection in the presence of rotation and a magnetic field: A heuristic theory. *Geophys. Astrophys. Fluid Dyn.* **12**, 139–169 (1979).
75. A. P. Ingersoll, D. Pollard, Motion in the interiors and atmospheres of Jupiter and Saturn: Scale analysis, anelastic equations, barotropic stability criterion. *Icarus* **52**, 62–80 (1982).
76. S. Sakai, The horizontal scale of rotating convection in the geostrophic regime. *J. Fluid Mech.* **333**, 85–95 (1997).
77. K. Julien, E. Knobloch, J. Werne, A new class of equations for rotationally constrained flows. *Theor. Comput. Fluid Dyn.* **11**, 251–261 (1998).
78. M. Sprague, K. Julien, E. Knobloch, J. Werne, Numerical simulation of an asymptotically reduced system for rotationally constrained convection. *J. Fluid Mech.* **551**, 141 (2006).
79. K. Julien, E. Knobloch, A. M. Rubio, G. M. Vasil, Heat transport in low-Rossby-number Rayleigh-Bénard convection. *Phys. Rev. Lett.* **109**, 254503 (2012).
80. S. Stellmach *et al*., Approaching the asymptotic regime of rapidly rotating convection: Boundary layers versus interior dynamics. *Phys. Rev. Lett.* **113**, 254501 (2014).
81. K. Julien *et al*., A nonlinear model for rotationally constrained convection with Ekman pumping. *J. Fluid Mech.* **798**, 50–87 (2016).
82. A. J. Barker, A. M. Dempsey, Y. Lithwick, Theory and simulations of rotating convection. *Astrophys. J.* **791**, 13 (2014).
83. L. G. Ireland, M. K. Browning, The radius and entropy of a magnetized, rotating, fully convective star: Analysis with depth-dependent mixing length theories. *Astrophys. J.* **856**, 132 (2018).
84. C. Guervilly, P. Cardin, N. Schaeffer, Turbulent convective length scale in planetary cores. *Nature* **570**, 368–371 (2019).
85. E. H. Anders, C. M. Manduca, B. P. Brown, J. S. Oishi, G. M. Vasil, Predicting the rossby number in convective experiments. *Astrophys. J.* **872**, 138 (2019).
86. L. K. Currie, A. J. Barker, Y. Lithwick, M. K. Browning, Convection with misaligned gravity and rotation: Simulations and rotating mixing length theory. *Mon. Not. R. Astron. Soc.* **493**, 5233–5256 (2020).
87. A. S. Jermyn, S. M. Chitre, P. Lesaffre, C. A. Tout, Convective differential rotation in stars and planets. I. Theory. *Mon. Not. R. Astron. Soc.* **498**, 3758–3781 (2020).
88. N. H. Brummell, N. E. Hurlburt, J. Toomre, Turbulent compressible convection with rotation. I. Flow structure and evolution. *Astrophys. J.* **473**, 494–513 (1996).
89. N. H. Brummell, N. E. Hurlburt, J. Toomre, Turbulent compressible convection with rotation. II. Mean flows and differential rotation. *Astrophys. J.* **493**, 955–969 (1998).
90. N. H. Brummell, T. L. Clune, J. Toomre, Penetration and overshooting in turbulent compressible convection. *Astrophys. J.* **570**, 825–854 (2002).
91. L. K. Currie, S. M. Tobias, Mean flow generation in rotating anelastic two-dimensional convection. *Phys. Fluids* **28**, 017101 (2016).
92. T. P. Larson, J. Schou, Global-mode analysis of full-disk data from the Michelson doppler imager and the helioseismic and magnetic imager. *Sol. Phys.* **293**, 29 (2018).
93. S. A. Balbus, H. Latter, N. Weiss, Global model of differential rotation in the sun. *Mon. Not. R. Astron. Soc.* **420**, 2457–2466 (2012).
94. A. S. Brun, H. M. Antia, S. M. Chitre, Is the solar convection zone in strict thermal wind balance? *Astron. Astrophys.* **510**, A33 (2010).
95. L. I. Matilsky, B. W. Hindman, J. Toomre, Revisiting the sun's strong differential rotation along radial lines. *Astrophys. J.* **898**, 111 (2020).
96. H. Hotta, M. Rempel, T. Yokoyama, Large-scale magnetic fields at high Reynolds numbers in magnetohydrodynamic simulations. *Science* **351**, 1427–1430 (2016).
97. H. Hotta, Breaking Taylor-Proudman balance by magnetic fields in stellar convection zones. *Astrophys. J.* **860**, L24 (2018).
98. A. M. Rubio, K. Julien, E. Knobloch, J. B. Weiss, Upscale energy transfer in three-dimensional rapidly rotating turbulent convection. *Phys. Rev. Lett.* **112**, 144501 (2014).
99. K. Julien, E. Knobloch, M. Plumley, Impact of domain anisotropy on the inverse cascade in geostrophic turbulent convection. *J. Fluid Mech.* **837**, R4 (2018).
100. B. Favier, C. Guervilly, E. Knobloch, Subcritical turbulent condensate in rapidly rotating Rayleigh–Bénard convection. *J. Fluid Mech.* **864**, R1 (2019).
101. C. Guervilly, D. W. Hughes, C. A. Jones, Large-scale vortices in rapidly rotating Rayleigh–Bénard convection. *J. Fluid Mech.* **758**, 407–435 (2014).
102. L. A. Couston, D. Lecoanet, B. Favier, M. L. Bars, Shape and size of large-scale vortices: A generic fluid pattern in geophysical fluid dynamics. *Phys. Rev. Res.* **2**, 023143 (2020).
103. M. L. DeRosa, P. A. Gilman, J. Toomre, Solar multiscale convection and rotation gradients studied in shallow spherical shells. *Astrophys. J.* **581**, 1356–1374 (2002).
104. G. M. Vasil, D. Lecoanet, K. J. Burns, J. S. Oishi, B. P. Brown, Tensor calculus in spherical coordinates using Jacobi polynomials. Part I. Mathematical analysis and derivations. *J. Comput. Phys. X* **3**, 100013 (2019).
105. D. Lecoanet, G. M. Vasil, K. J. Burns, B. P. Brown, J. S. Oishi, Tensor calculus in spherical coordinates using jacobi polynomials. Part II. Implementation and examples. *J. Comput. Phys. X* **3**, 100012 (2019).
106. B. W. Hindman, N. A. Featherstone, K. Julien, Morphological classification of the convective regimes in rotating stars. *Astrophys. J.* **898**, 120 (2020).
107. T. S. Metcalfe *et al*., The evolution of rotation and magnetic activity in 94 aqr aa from asteroseismology with TESS. *Astrophys. J.* **900**, 154 (2020).